Research Article

For reprint orders, please contact: reprints@futuremedicine.com

Nanomedicine

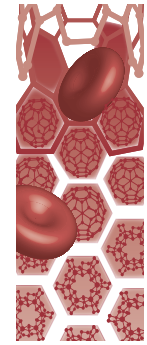

Efficacy and pharmacokinetics of a modified acid-labile docetaxel-PRINT® nanoparticle formulation against non-small-cell lung cancer brain metastases

Aim: Particle Replication in Nonwetting Templates (PRINT®) PLGA nanoparticles of docetaxel and acid-labile C2-dimethyl-Si-Docetaxel were evaluated with small molecule docetaxel as treatments for non-small-cell lung cancer brain metastases. **Materials & methods:** Pharmacokinetics, survival, tumor growth and mice weight change were efficacy measures against intracranial A549 tumors in nude mice. Treatments were administered by intravenous injection. **Results:** Intracranial tumor concentrations of PRINT-docetaxel and PRINT-C2-docetaxel were 13- and sevenfold greater, respectively, than SM-docetaxel. C2-docetaxel conversion to docetaxel was threefold higher in intracranial tumor as compared with nontumor tissues. PRINT-C2-docetaxel increased median survival by 35% with less toxicity as compared with other treatments. **Conclusion:** The decreased toxicity of the PRINT-C2-docetaxel improved treatment efficacy against non-small-cell lung cancer brain metastasis.

First draft submitted: 6 April 2016; Accepted for publication: 8 June 2016; Published online: 26 July 2016

Keywords: acid-labile docetaxel prodrug • blood–brain barrier • Particle Replication in Non-wetting Templates (PRINT)® PLGA nanoparticle

Maria Sambade[1], Allison Deal[1], Allison Schorzman[1,2], J Christopher Luft[1], Charles Bowerman[1,3], Kevin Chu[1,2], Olga Karginova[1,4], Amanda Van Swearingen[1], William Zamboni[1,2], Joseph DeSimone[1,3] & Carey K Anders*[,1,4]

[1]Lineberger Comprehensive Cancer Center, Chapel Hill, NC, USA
[2]Department of Pharmacology, University of North Carolina, Chapel Hill, NC, USA
[3]Department of Chemistry, University of North Carolina, Chapel Hill, NC, USA
[4]Department of Medicine, University of North Carolina, Chapel Hill, NC, USA
*Author for correspondence:
Tel.: +1 919 966 5874
Fax: +1 919 966 6735
carey_anders@med.unc.edu

Lung cancer, 80% comprised of non-small-cell lung cancer (NSCLC), is one of the leading causes of cancer worldwide and the USA [1–3]. Lung cancer is the most common primary tumor responsible for brain metastases [19]. Among those diagnosed with NSCLC, 20–50% of patients will develop metastatic brain disease [2], 10% with brain metastases at initial diagnosis [4] and another 30% later in their disease course following standard therapies.

Despite multimodality therapy with combinations of surgery, radiation therapy and chemotherapy, median survival remains less than one year for NSCLC brain metastatic patients [1,2]. NSCLC brain metastases are generally nonresponsive to first-line, single agent platinum-based chemotherapy [2,5]. Docetaxel (Taxotere®) is a standard second line systemic chemotherapy for NSCLC brain metastases [2].

As brain metastasis recurrence is common among patients with advanced NSCLC, optimizing the passage of anticancer agents across the blood–brain barrier, increasing chemotherapeutic concentrations in intracranial and extracranial tumors and decreasing systemic toxicities are important considerations to improve treatment of this disease. Newer delivery techniques, like nanoparticles and carrier-mediated technologies, have illustrated these advantages in the setting of intracranial cancer [6–10]. Clinically, activity of nanoparticle-based systemic therapy has been illustrated in the setting of breast cancer brain metastases, another solid tumor type where brain metastasis recurrence is common [11].

While several studies have shown the superiority of nanoparticle anticancer agents in intracranial malignancies over standard formulations, the mechanism underlying this

Future Medicine part of fsg

observation has yet to be fully elucidated [6–12]. The working hypothesis has been that prolonged exposure to anticancer agents afforded by nanoparticle technology may increase passage of small molecules across the 'blood tumor barrier,' a barrier potentially compromised by the presence of tumor [12].

Particle Replication in Nonwetting Templates (PRINT)® of poly-(lactic acid-co-glycolic acid)-docetaxel

PRINT-poly(lactic acid-co-glycolic acid) (PLGA) nanoparticle formulations of docetaxel have shown superior pharmacokinetic and efficacy profiles over that of standard small molecule docetaxel (SM-docetaxel) in an extracranial NSCLC xenograft model [13]. Given the superior intracranial pharmacokinetic and efficacy profiles for nanoparticle anticancer agents in solid tumors, and the activity of docetaxel in NSCLC, we hypothesized that PRINT PLGA-docetaxel formulations would increase docetaxel concentrations in intracranial tumors and decrease intracranial tumor growth as compared with SM-docetaxel, thereby improving survival. We expected that the acid labile C2-prodrug PRINT® PLGA formulation (PRINT-C2-docetaxel), which should be specifically activated by an acidic tumor microenvironment, would increase efficacy with decreased toxicity over PRINT-PLGA docetaxel (PRINT-docetaxel).

Methods & materials

Pharmacologic agents

Small molecule docetaxel (SM-docetaxel; Taxotere) was obtained from the University of North Carolina Hospitals Pharmacy. A single step reaction of docetaxel with chlorodimethylethylsilane was performed to generate the C2′ alcohol of taxane, the silyl ether docetaxel prodrug C2, as previously described [13]. PRINT-C2-docetaxel and PRINT-docetaxel nanoparticles were fabricated as previously described, to form the same sized cylindrical particles of PLGA polymer with a diameter of 80 nm and height of 320 nm, with similar drug loading [13,15–18]. Briefly, a thin film of PLGA and Docetaxel or C2-Docetaxel was deposited on a 6″ × 12″ sheet of PET (poly[ethylene terephthalate]) by spreading 150 µl of a 10 mg/ml PLGA and 10 mg/ml docetaxel or C2-docetaxel chloroform solution using a # 5 Mayer Rod (R.D. Specialties). The solvent was evaporated with heat. The PET sheet with the film was then placed in contact with the patterned side of a mold and passed through heated nips (ChemInstruments Hot Roll Laminator) at 130°C and 80 psi. The mold was split from the PET sheet as they both passed through the hot laminator. The patterned side of the mold was then placed in contact with a sheet of PET coated with 2000 g/mol PVOH (poly[vinyl alcohol]). This was then passed through the hot laminator to transfer the particles from the mold to the PET sheet. The mold was then peeled from the PET sheet. The particles were removed by passing the PVOH coated PET sheet through motorized rollers and applying water to dissolve the PVOH to release the particles. To remove excess PVOH, the particles were purified and then concentrated by tangential flow filtration (Spectrum Labs).

A549 intracranial xenograft studies

All animal studies protocols were approved by the University of North Carolina, Chapel Hill Institutional Animal Care and Use Committee, executed by the UNC Animal Studies Core, and performed as previously described [6,13,14]. Briefly, A549-luc-c8, acquired from Caliper Life Sciences (P/N 119266, Perkin Elmer), was propagated in culture in DMEM 10% FBS supplemented with G418 (200 µg/ml). For intracranial injections, cells were harvested in log-phase growth and suspended with 5% methylcellulose in culture media. Eight to ten week Foxn1 *nu/nu* mice (UNC Animal Studies Core) were implanted with 200,000 cells/5 uls of cell suspension through stereotactic intracranial injection in the right striatum. Animal weights were collected from injection to sacrifice three-times weekly. To determine tumor volumes, mice were anesthetized, injected intraperitoneally with D-Luciferin dissolved in PBS (150 mg/kg; Caliper Life Sciences, MA, USA), then imaged by IVIS Lumina camera (Caliper Life Sciences). Images were analyzed with Living Image 4.0 software (Caliper Life Sciences). All values were corrected for background and recorded as photons/second.

For pharmacokinetic studies, tumors were grown to greater than 2 mm in diameter correlating with bioluminescence signal which occurred between 30 and 40 days post-intracranial injection of tumor cells. The following treatments were given once by IV a) SM-docetaxel at 15 mg/kg, b) PRINT-docetaxel at 30 mg/kg, c) PRINT® C2- docetaxel at 30 mg/kg. These doses were in SM-docetaxel equivalents and below previously determined maximum tolerated doses for nontumor bearing nude mice (nu/nu) [13]. Tumors were collected at n = 3 per time point per treatment, as shown in Figure 1. PBS controls (n = 2) were collected as negative controls for pharmacokinetic analysis. Figures were generated using GraphPad Prism 6.

For efficacy studies, mice were grouped between 21 and 28 days post-injection of tumor cells by intracranial bioluminescence signals, (nu/nu) [13]. Tumor growth by bioluminescence was monitored weekly. Mice weights were collected three-times a week throughout efficacy

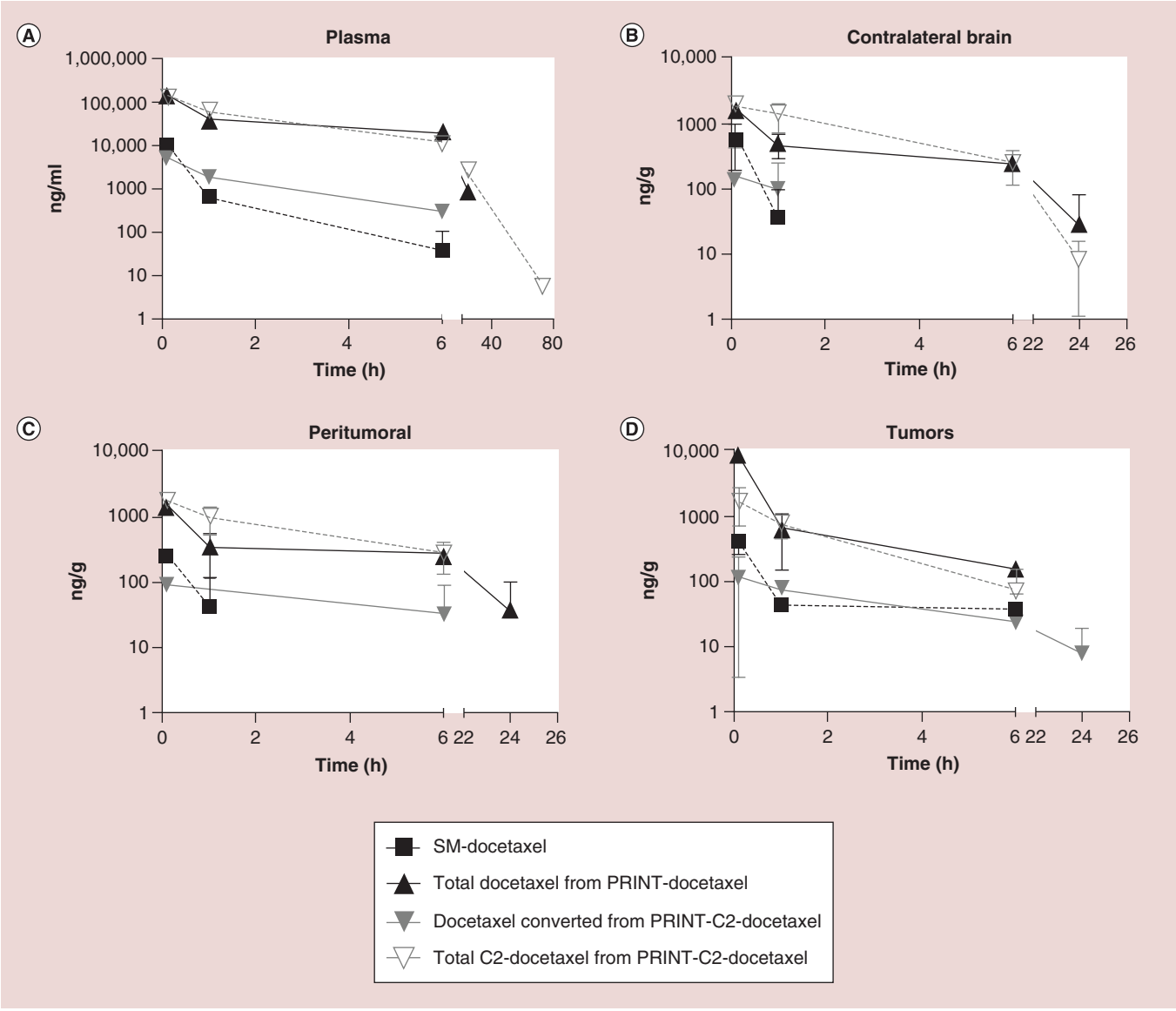

Figure 1. Individual and mean concentrations of docetaxel and C2-docetaxel after administration of SM-docetaxel at 15 mg/kg, PRINT-docetaxel at 30 mg/kg, or PRINT-C2-docetaxel at 30 mg/kg docetaxel, by IV × 1 to nu/nu mice bearing intracranial A549 tumors. Concentrations below the lower limit of quantitation (LLOQ) are not shown. Pharmacokinetic analysis included **(A)** plasma; **(B)** contralateral brain; **(C)** peritumoral brain; and **(D)** intracranial tumors.

studies. Two separate efficacy studies were performed and experiments combined, for n > 9/group. Tumor volume change and weight change figures were generated using GraphPad Prism 6, with groups normalized to a baseline value from initial tumor volumes or initial weights at grouping.

Pharmacokinetics analysis

After sacrifice, plasma, contralateral brain, intracranial tumor and the peritumor brain tissue consisting of the 2 mm perimeter surrounding intracranial tumor were collected and snap frozen in liquid nitrogen. The associations between injected agents (SM-docetaxel, PRINT-docetaxel and PRINT-C2-docetaxel) and downstream pharmacokinetic analytes (docetaxel and C2-docetaxel) are summarized in Table 1. Docetaxel was measured in all samples after administration of SM-docetaxel, PRINT-docetaxel and PRINT-C2-docetaxel, as previously described [13]. The analysis of docetaxel in PRINT-docetaxel samples measured nanoparticle-encapsulated + released docetaxel. The analysis of docetaxel from PRINT-C2-docetaxel samples measured converted C2-docetaxel, released from nanoparticle-encapsulation [13]. C2-docetaxel was measured in all samples after administration of PRINT-C2-docetaxel, representative of nanoparticle-

Table 1. Pharmacokinetic analytes of injected agents.

Injected agent	Docetaxel	C2-docetaxel
SM-Docetaxel	Free	NA
PRINT-Docetaxel	Encapsulated + free	NA
PRINT-C2-Docetaxel	Free converted	Encapsulated + free

encapsulated + released C2-docetaxel prodrug. All samples were analyzed using liquid chromatography tandem mass spectroscopy (LC-MS/MS), as previously described [13].

Data analysis & statistical methods

Generally, all data analysis and statistical methods were performed as previously described [6,13,14,17].

Pharmacokinetic analysis

Pharmacokinetic data were analyzed by noncompartmental methods using WinNonLin Professional Edition version 6.1 (Pharsight Corp, NC, USA). The area under the concentration curve (AUC) versus time was calculated from 0 to t_{last}. The conversion of PRINT-C2-docetaxel prodrug to active docetaxel was calculated from the PRINT-C2-docetaxel AUCs as follows: [AUC_doctaxel/(AUC_C2-docetaxel+AUC_docetaxel)]*100 [13].

Efficacy

The Kaplan–Meier method and Log rank test were used to estimate and compare median survival between treatment groups. Median survivals, along with their 95% confidence intervals, and Log-rank test p-values were reported.

Tumor volume changes & mouse weight change analysis

Both fold change in tumor volumes and mice weight over time were determined relative to treatment start date. Linear mixed models, with a random intercept and slope, were used to evaluate changes over time, overall and between groups. SAS statistical software, v9.3, was used for these analyses (NC, USA).

Results

Pharmacokinetics of SM-docetaxel, PRINT-docetaxel & PRINT-C2-docetaxel in intracranial NSCLC tumor-bearing nude mice

To demonstrate that PRINT-docetaxel and PRINT-C2-docetaxel formulations can increase intracranial tissue exposure to docetaxel, a pharmacokinetic study was performed using the A549 human non-small-cell lung cancer (NSCLC) brain metastases xenograft murine model with administration of SM-docetaxel, PRINT-docetaxel and PRINT-C2-docetaxel. This KRAS-activated NSCLC background was shown to be responsive to both PRINT-docetaxel formulations in a subcutaneous tumor model [13].

Table 1 summarizes the association of analytes (docetaxel or C2-docetaxel) with chemotherapeutic agents injected (SM-docetaxel, PRINT-docetaxel, PRINT-C2-docetaxel). Figure 1 shows the pharmacokinetic profile of docetaxel after single dose administration of SM-docetaxel, PRINT-docetaxel, PRINT-C2-docetaxel, in plasma, contralateral brain, peritumoral brain and intracranial tumor.

In each tissue analyzed, the nanoparticle formulations achieved higher exposures of drug in tumors compared with SM-docetaxel. Both PRINT-docetaxel and PRINT-C2-docetaxel formulations, measured by docetaxel and C2-docetaxel respectively, were detected 24 h or later after administration in plasma and contralateral brain. Docetaxel from SM-docetaxel or converted C2-docetaxel prodrug were detectable for 6 h after administration of SM-docetaxel or PRINT-C2-docetaxel in plasma and undetectable 2 h after administration in contralateral brain. In peritumoral brain, docetaxel from PRINT-docetaxel was present at 24 h after administration, as compared with SM-docetaxel, C2-docetaxel from PRINT-C2-docetaxel, or docetaxel from converted C2-docetaxel, all undetected beyond 6 h after administration. Docetaxel from the converted C2- prodrug was detected in intracranial tumors for up to 24 h, as compared with SM-docetaxel, C2-docetaxel prodrug from PRINT-C2-docetaxel, or docetaxel from PRINT-docetaxel, all undetectable after 6 h.

While AUCs were similar in contralateral brain, peritumoral brain and intracranial tumor, the Cmax for the docetaxel converted from PRINT-C2-docetaxel prodrug was three- to fourfold lower than SM-docetaxel in these intracranial tissues tested. These data are summarized in Table 2. These data also show a greater than threefold increased conversion of the released C2-docetaxel prodrug in intracranial tumor (10.9%) as compared with plasma, contralateral brain or peritumoral brain (3% or less). These data demonstrate that docetaxel from both PRINT-docetaxel formulations cross the blood–brain barrier and accumulate in intracranial tumors.

PRINT-C2-docetaxel increases survival as compared with docetaxel & PRINT-docetaxel in an intracranial model of NSCLC

The efficacy of PRINT-docetaxel formulations as compared with SM-docetaxel were evaluated in the NSCLC brain metastases model A549 (Figure 2). Analysis of tumor growth rates by bioluminescence is summarized in Figure 2A. The growth rate of vehicle-control treated tumors was significantly higher from all treatment groups from start of treatment (day 21) through day 60 ($p < 0.0001$); there were no differences in tumor growth rate between all other treatment groups ($p > 0.7$).

Comparison of median survivals by treatment (Figure 2B) demonstrated that the PRINT-C2-docetaxel significantly improved survival by greater than 35% as compared with other treatment arms. Median survival in response to PRINT-C2-docetaxel was 90 days (95% CI: 70–103) as compared with vehicle control (61 days (95% CI: 50–68), SM-docetaxel (66.5 days (95% CI: 57–86), and PRINT-docetaxel (58 days [95% CI: 37–79], overall p-value: $p = 0.1556$). These data illustrate that while all treatments decreased tumor burden and slowed tumor growth rates, only treatment with the PRINT-C2-docetaxel prodrug improved survival.

Figure 3 demonstrates that mice treated with PRINT-C2-docetaxel therapy exhibited stable weight during the first 6 weeks of therapy. Mice in the other treatment or control groups exhibited weight loss during the first 6 weeks of therapy, significantly different than that of PRINT-C2-docetaxel ($p < 0.003$). The weight loss in the PBS group followed closely with tumor burden as expected. However, in SM-docetaxel and PRINT-docetaxel groups, weight loss did not correspond with tumor burden and steadily decreased with treatment number. This demonstrates that PRINT-C2-docetaxel was effective in reducing intracranial tumor burden without significant toxicity during the first 6 weeks of treatment resulting in improved overall survival.

Discussion

Brain metastases, increasing in frequency as therapeutics for advanced extracranial cancer progress and evolve, require novel therapeutic approaches. Therapies for brain metastases should effectively target tumor tissue in the brain at concentrations high enough to induce tumor cell death and/or stabilize disease, while minimizing normal intracranial and extracranial toxicities, thereby increasing survival and quality of life.

This work shows that intravenous injections of PRINT PLGA nanoparticle formulations of docetaxel and the prodrug C2-docetaxel deliver docetaxel to intracranial tumors and exhibit antitumor activity against an orthotopic model of *KRAS*-NSCLC brain metastases. AUC analysis illustrates that delivery of released docetaxel from PRINT-docetaxel or the C2-docetaxel prodrug via PRINT-C2-docetaxel nanoparticles was higher than that of SM-docetaxel in intracranial tumors, 13-fold for PRINT-docetaxel and sevenfold for PRINT-C2-docetaxel (Table 2). Moreover, nanoparticles were detected in plasma for up to 72 h (Figure 1). In comparison to prior studies with PRINT-docetaxel formulations, the AUC of the intracranial tumor for each treatment were at lower levels than those described in the A549 tumor flank model (4885 vs 60,858 for PRINT-docetaxel; 2634 vs 26,799 for PRINT-C2-docetaxel; 372 vs 73,222 for SM-docetaxel), although plasma AUCs for all treatments were higher in this study as compared with the flank study (326,352 vs 79,192 for PRINT-docetaxel; 360,281 vs 227,735 for PRINT-C2-docetaxel; 4742 vs 1227 for SM-docetaxel) for similar dosing concentrations [13]. As compared with flank studies [13], intra-

Table 2. Pharmacokinetic parameters.

Injected agent	Taxotere		PRINT-docetaxel		PRINT-C2-dimethyl-Si-docetaxel				Conversion of C2-docetaxel to docetaxel
Analyte	Docetaxel		Docetaxel		C2-docetaxel		Docetaxel		
	AUC ng/ml*h	C_{max} ng/ml	AUC ng/ml*h	C_{max} ng/ml	AUC ng/ml*h	C_{max} ng/ml	AUC ng/ml*h	C_{max} ng/ml	
Plasma	4742	10,256	326,352	147,694	360,281	125,535	7683	5475	2.1%
Contralateral brain	189	535	4274	1516	5892	1772	109	90	1.8%
Peri-tumoral brain	118	252	2546	1516	4011	1740	125	89	3.0%
Brain tumor	372	394	4885	8558	2634	1704	321	120	10.9%

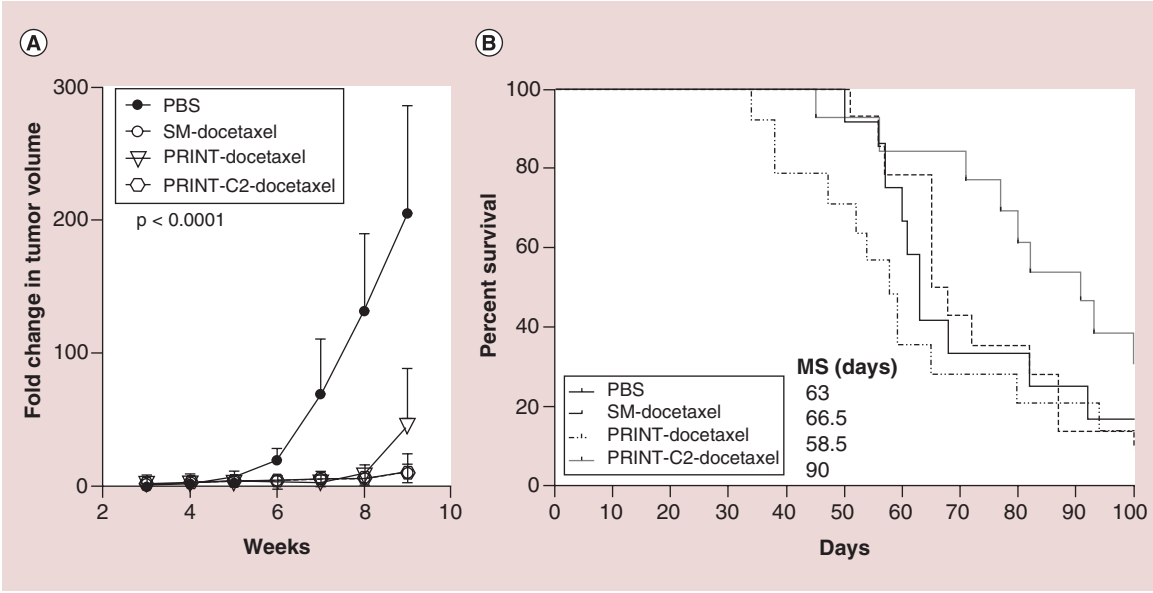

Figure 2. All docetaxel therapies decrease tumor burden, but PRINT-C2-docetaxel improves survival. (A) The tumor volume changes among treatment groups are similar to each other, but all are significantly better than the PBS control ($p < 0.0001$). **(B)** PRINT-C2-docetaxel improved median survival by greater than 35% over all other treatments and PBS.

cranial tumor AUCs were an order of magnitude lower for each treatment observed, suggesting a drug delivery issue, likely related to the blood–brain barrier [12,20].

The silyl ether C2′ alcohol of docetaxel was generated to produce an acid labile docetaxel prodrug that could specifically target the acidic environments of cancer cells. The applicability of the acid labile chemistry of silyl ethers as anticancer prodrugs was previously demonstrated with gemcitabine [23]. In this case, lower pH increased both prodrug release and conversion from the PRINT nanoparticle. Consistent with the model, PRINT-C2-docetaxel had an increased conversion of 10.9% in intracranial tumors, as compared with 2.1, 1.8 and 3.0% in plasma, contralateral and peritumor environments, respectively. The C2-docetaxel conversion rate in intracranial tumors is lower than in the flank model (32.5 vs 10.9%), but at a similar conversion value as described for liver [13], and is within the range of other clinically relevant prodrug strategies. We did not determine a mechanism for the decrease in prodrug conversion in the intracranial tumors, which could include mass action effects due to lower concentrations of C2-docetaxel in intracranial versus extracranial tumors or a difference in tumor biology based on the contributing brain tissue environment.

While all treatment arms decreased tumor burden and slowed intracranial growth rates by bioluminescence imaging, the PRINT-C2-docetaxel increased median survival, by greater than 35%, as compared with all other treatment arms. We hypothesize that the efficacy of the PRINT-C2-docetaxel is due to decreases in toxicity [13]. This is supported by the following evidence: 1) Pharmacodynamics from previous studies show that PRINT-C2-docetaxel has slower release kinetics as compared with PRINT-docetaxel due to the increased lipophilicity of C2-docetaxel as compared with docetaxel; 50% of the PRINT-C2-docetaxel is released at 24 h as compared with less than 6 h with PRINT-docetaxel cargo. Additionally, C2-docetaxel has an 8 h half-life for conversion to docetaxel in PBS [13]. This demonstrates that the longer retention of C2-docetaxel in the nanoparticle, with an added conversion rate to docetaxel, delays active drug release, minimizing toxicity. 2) In this study, the docetaxel from the release and conversion of the PRINT encapsulated C2-docetaxel has a lower Cmax in plasma than the SM-docetaxel, although converted docetaxel from PRINT-C2-docetaxel was found 24 h after injection in contrast to SM-docetaxel or PRINT-docetaxel in intracranial tumor. This supports previous pharmacodynamics analysis [13] and is consistent with the hypothesis that PRINT-C2-docetaxel would be less toxic than SM-docetaxel in these studies. 3) While all docetaxel treatments decreased tumor burden (Figure 2A), only the PRINT-C2-docetaxel increased median survival as compared with all other treatment arms (Figure 2B). 4) Docetaxel treatment is consistently associated with neutropenia, which may be minimized by PRINT-C2-docetaxel. In previous studies [13], 4 days after the sixth intravenous dose of 20 mg/kg, animals treated with PRINT-C2-docetaxel had PBS control levels of white blood cells, and twice the white blood cell levels

as SM-docetaxel treated animals, at equimolar dosing. 5) With regards to median survival and the 60 days post-intracranial injection with six doses of treatment, the SM-docetaxel, PRINT-docetaxel and PBS control groups showed weight decline that correlated to time of death. However, tumor burden in SM-docetaxel and PRINT-docetaxel was significantly decreased as compared with PBS controls, supporting treatment-specific toxicity. Mice treated with the PRINT-C2-docetaxel showed no change in weight during this timeframe and decreased tumor burden. This was also consistent with previous studies [13].

Targeting drug to tumors through nanoparticle delivery methodologies is a promising strategy to increase tumor cytotoxicity and decrease drug-associated toxicities. Encapsulated cargo has a different pharmacodynamic profile than free drug and takes on the pharmacokinetics of its carrier. This results in increased systemic half-life of the drug, changes in the drug tissue distribution and increased drug-tumor exposure with less systemic toxicity [6,9,13,17]. In this manner, nanoparticle encapsulation generates a prodrug of the free drug cargo [6]. However, in this study, simply changing drug distribution and increasing target dosing by encapsulating free chemotherapeutic drug (i.e., docetaxel) did not balance decreased systemic toxicity to support extended survival. The mechanism supporting decreased PRINT-C2-docetaxel toxicity may include the longer half-life of cargo release as compared with PRINT-docetaxel (24 h vs <6 h at pH 7.4), as well as the timing and specificity of the target tissue activation [13].

Target tissue activation of the C2-docetaxel prodrug is modeled to occur through ethyl-dimethyl-silyl-ether docetaxel protonation and hydrolysis, resulting in docetaxel release. This reaction proceeds in acidic environments like tumors, without enzymatic activity [13]. Cancer cells' dependency for anaerobic metabolism generates an acidic extracellular microenvironment and intracellular endocytic and lysosomal vesicular network. This increases activation of acid-labile molecules for anticancer therapy with some tumor specificity. This strategy is being vigorously tested in the context of acid labile nanoparticles, targeting agents and prodrugs like C2-docetaxel [21,22]. This study introduces the application of the acid labile chemistry of silyl ethers tagged chemotherapeutics as a targeting agent for intracranial tumors.

Conclusion

We conclude that PRINT nanoparticles of docetaxel can enter and inhibit growth of human intracranial

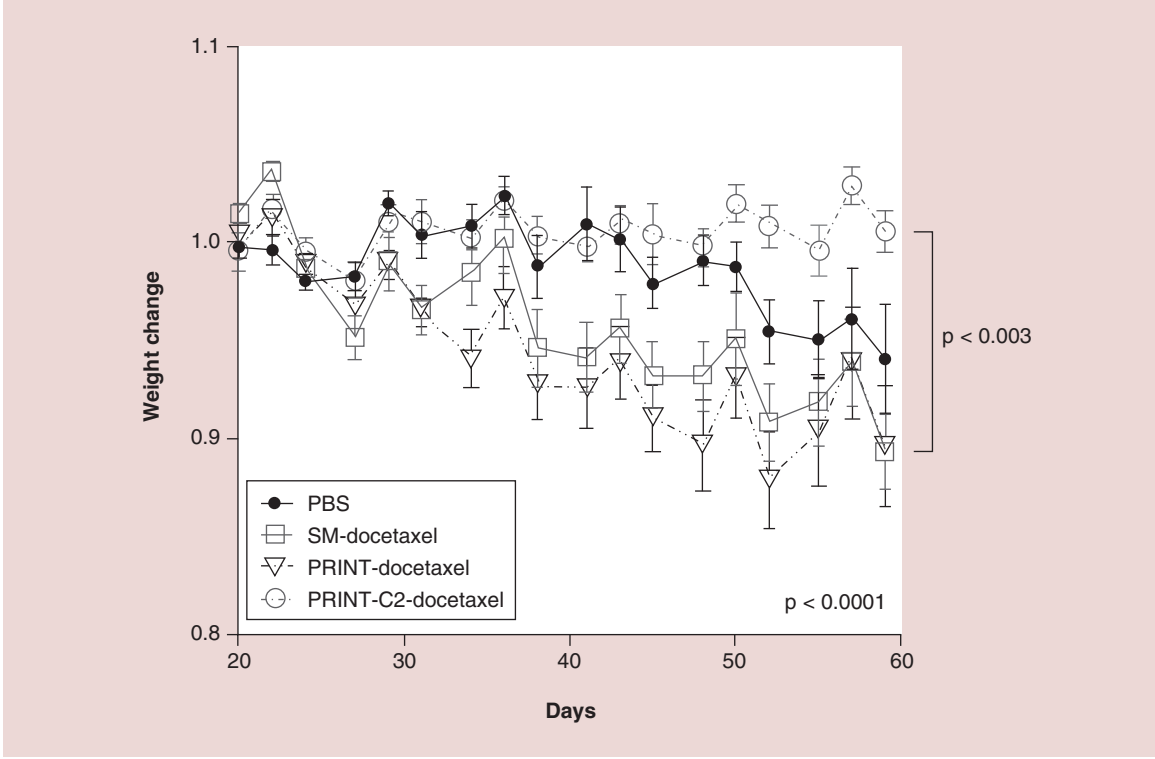

Figure 3. PRINT-C2-Docetaxel minimizes docetaxel toxicity as measured by average weight change. Weight change is summarized for first 6 weeks of treatment. Weight change between groups was found to be statistically significant from each other ($p < 0.0001$), with PRINT-C2-docetaxel different statistically from SM-docetaxel and PRINT-docetaxel ($p < 0.003$).

tumors in a murine xenograft model of NSCLC. We show that intravenous administrations of PRINT-C2-docetaxel prodrug are more efficacious than either free docetaxel or PRINT-docetaxel against a brain metastasis model of NSCLC. We conclude that PRINT-C2-docetaxel increases survival by decreasing systemic toxicities, through slower chemotherapeutic release and the targeted conversion of the prodrug in the intracranial tumor environment. We confirm that decreasing the systemic toxicity of chemotherapeutics is an important adjunct treatment strategy against intracranial cancers.

Disclaimer

The content is solely the responsibility of the authors and does not necessarily represent the official views of the National Cancer Institute or the National Institutes of Health.

Acknowledgements

C Bowerman is currently a research associate for Moderna Therapeutics (MA, USA). K Chu is currently a research associate for GSK Pharmaceuticals, Research Triangle Park (NC, USA). O Karginova is currently a research associate in the Department of Hematology and Oncology, University of Chicago (IL, USA). Additionally, the authors would like to thank Liquidia Technologies for providing PRINT® molds used in the fabrication of nanoparticles.

Financial & competing interests disclosure

The authors of this manuscript receive uncompensated research funding from Novartis, Sanofi, toBBB, GERON, Angiochem, Merrimack, PUMA, Lily, Merck, Oncothyreon. CK Anders serves in an uncompensated advisory role for Novartis, Sanofi, toBBB, GERON, angiochem, Merrimack, Lily, Genentech, Nektar, Kadmon. The project described was supported by grant number K23CA157728 (CK Anders) from the National Cancer Institute. Research was supported by the 2010 Breast Cancer Research Foundation-AACR Grant for Translational Breast Cancer Research, grant number 10-60-26-ANDE (CK Anders). CK Anders is a Damon Runyon Clinical Investigator, supported (in part) by the Damon Runyon Cancer Research Foundation (CI-64-12). Funding also came from the Lineberger Comprehensive Cancer Center University of North Carolina SPORE Career Development Award, 5P50CA058223 (SPORE; CK Anders), University Cancer Research Fund and the Carolina Center for Cancer Nanotechnology Excellence (U54CA151652; JC Luft, C Bowerman, K Chu, JM DeSimone). The authors have no other relevant affiliations or financial involvement with any organization or entity with a financial interest in or financial conflict with the subject matter or materials discussed in the manuscript apart from those disclosed.

No writing assistance was utilized in the production of this manuscript.

Ethical conduct of research

The authors state that they have obtained appropriate institutional review board approval or have followed the principles outlined in the Declaration of Helsinki for all human or animal experimental investigations. In addition, for investigations involving human subjects, informed consent has been obtained from the participants involved.

Executive summary

Background

- Nanoparticle formulations of PRINT-docetaxel and PRINT acid labile C2-docetaxel prodrug have been shown to be more effective than free drug against the A549 NSCLC subcutaneous xenograft model.

Results

- Given at similar molar doses, docetaxel and C2-prodrug docetaxel from PRINT-nanoparticle formulations were found in intracranial tumor and brain tissues at greater than sevenfold higher concentrations than SM-docetaxel at all time points.
- The AUCs for docetaxel from converted C2 prodrug and SM-docetaxel were similar in intracranial tissues tested; the Cmax for C2 prodrug was three- to fourfold lower than SM- docetaxel.
- Conversion of the acid-labile C2 prodrug to docetaxel was highest in intracranial tumor tissue, 10.9% as compared with 2.1% in plasma, 1.8% in contralateral brain and 3.0% in peritumoral brain.
- All docetaxel treatments significantly decreased tumor burden as compared with control during the first 6 weeks of treatment ($p < 0.0001$).
- The PRINT C2-docetaxel prodrug formulation treatment increased median survival to 90 days, as compared with 61 days for control, 58.5 days with PRINT-docetaxel and 66.5 days with SM-docetaxel.
- PRINT C2-docetacel was less toxic by measures of weight change during the first 6 weeks of treatment.

Discussion

- Acid-labile PRINT C2-prodrug nanoparticle, because of improved tumor specificity resulting in decreased systemic toxicity, had a superior efficacy as compared with SM-docetaxel and PRINT-docetaxel against a NSCLC brain metastases model.
- The combination of PRINT PLGA nanoparticle technology with a tumor activated agent may be a useful anticancer therapeutic for intracranial tumors.

References

Papers of special note have been highlighted as: • of interest; •• of considerable interest

1 Yamanaka R. Medical management of brain metastases from lung cancer (Review). *Oncol. Rep.* 22(6), 1269–1276 (2009).

2 Reck M, Heigener DF, Mok T, Soria J-C, Rabe KF. Management of non-small-cell lung cancer: recent developments. *Lancet* 382(9893), 709–719 (2013).

3 National Cancer Institute. SEER Stat Fact Sheets: Lung and Bronchus Cancer. http://seer.cancer.gov/statfacts/html/lungb.html

4 Schuchert MJ, Luketich JD. Solitary sites of metastatic disease in non-small cell lung cancer. *Curr. Treat. Options Oncol.* 4(1), 65–79 (2003).

5 Lwin Z, Riess JW, Gandara D. The continuing role of chemotherapy for advanced non-small cell lung cancer in the targeted therapy era. *J. Thorac. Dis.* 5(Suppl. 5), S556–S564 (2013).

6 Anders CK, Adamo B, Karginova O *et al.* Pharmacokinetics and efficacy of PEGylated liposomal doxorubicin in an intracranial model of breast cancer. *PLoS ONE* 8(5), e61359 (2013).

• **Demonstration of the efficacy of nanoparticles loaded with chemotherapeutics against preclinical intracranial models of triple negative breast cancer.**

7 Zamboni WC, Strychor S, Joseph E *et al.* Plasma, tumor, and tissue disposition of STEALTH liposomal CKD-602 (S-CKD602) and nonliposomal CKD-602 in mice bearing A375 human melanoma xenografts. *Clin. Cancer Res.* 13(23), 7217–7223 (2007).

8 Walsh MD, Hanna SK, Sen J *et al.* Pharmacokinetics and antitumor efficacy of XMT-1001, a novel, polymeric topoisomerase I inhibitor, in mice bearing HT-29 human colon carcinoma xenografts. *Clin. Cancer Res.* 18(9), 2591–2602 (2012).

9 Siegal T, Horowitz A, Gabizon A. Doxorubicin encapsulated in sterically stabilized liposomes for the treatment of a brain tumor model: biodistribution and therapeutic efficacy. *J. Neurosurg.* 83(6), 1029–1037 (1995).

10 Koukourakis MI, Koukouraki S, Fezoulidis I *et al.* High intratumoural accumulation of stealth liposomal doxorubicin (Caelyx) in glioblastomas and in metastatic brain tumours. *Br. J. Cancer* 83(10), 1281–1286 (2000).

11 Linot B, Campone M, Augereau P *et al.* Use of liposomal doxorubicin-cyclophosphamide combination in breast cancer patients with brain metastases: a monocentric retrospective study. *J. Neurooncol.* 117(2), 253–259 (2014).

12 Lockman PR, Mittapalli RK, Taskar KS *et al.* Heterogeneous blood-tumor barrier permeability determines drug efficacy in experimental brain metastases of breast cancer. *Clin. Cancer Res.* 16(23), 5664–5678 (2010).

• **Demonstrates that intracranial tumors can have a compromised blood–brain barrier that allows increased chemotherapeutic penetrance as compared with brain, but less than extracranial tissues.**

13 Chu KS, Finniss MC, Schorzman AN *et al.* Particle replication in nonwetting templates nanoparticles with tumor selective alkyl silyl ether docetaxel prodrug reduces toxicity. *Nano Lett.* 14(3), 1472–1476 (2014).

•• **Demonstrates the efficacy of the PRINT-C2-Docetaxel prodrug against an extracranial model of A549.**

14 Karginova O, Siegel MB, Van Swearingen AED *et al.* Efficacy of carboplatin alone and in combination with ABT888 in intracranial murine models of BRCA-mutated and BRCA-wild-type triple-negative breast cancer. *Mol. Cancer Ther.* 14(4), 920–930 (2015).

15 Perry JL, Herlihy KP, Napier ME, DeSimone JM. PRINT: a novel platform toward shape and size specific nanoparticle theranostics. *Acc.Chem. Res.* 44(10), 990–998 (2011).

16 Gratton SEA, Ropp PA, Pohlhaus PD *et al.* The effect of particle design on cellular internalization pathways. *Proc. Natl Acad. Sci. USA* 105(33), 11613–11618 (2008).

17 Chu KS, Hasan W, Rawal S *et al.* Plasma, tumor and tissue pharmacokinetics of Docetaxel delivered via nanoparticles of different sizes and shapes in mice bearing SKOV-3 human ovarian carcinoma xenograft. *Nanomedicine* 9(5), 686–693 (2013).

• **Demonstrates the enhanced half-life and decreased clearance of the PRINT particle 320 × 80 nm used in this study.**

18 Enlow EM, Luft JC, Napier ME, DeSimone JM. Potent engineered PLGA nanoparticles by virtue of exceptionally high chemotherapeutic loadings. *Nano Lett.* 11(2), 808–813 (2011).

19 Owonikoko TK, Arbiser J, Zelnak A *et al.* Current approaches to the treatment of metastatic brain tumours. *Nat. Rev. Clin. Oncol.* 11(4), 203–222 (2014).

20 Connell JJ, Chatain G, Cornelissen B *et al.* Selective permeabilization of the blood–brain barrier at sites of metastasis. *J. Natl Cancer Inst.* 105(21), 1634–1643 (2013).

21 Liu J, Huang Y, Kumar A *et al.* pH-sensitive nano-systems for drug delivery in cancer therapy. *Biotechnol. Adv.* 32(4), 693–710 (2014).

22 Du J, Lane LA, Nie S. Stimuli-responsive nanoparticles for targeting the tumor microenvironment. *J. Control. Release* 219, 205–214 (2015).

• **Review of the use of the tumor microenvironment, including decreased pH and hypoxia, for anticancer therapy.**

23 Parrott MC, Finniss M, Luft JC *et al.* Incorporation and controlled release of silyl ether prodrugs from PRINT nanoparticles. *J. Am. Chem. Soc.* 134(18), 7978–7982 (2012).

•• **Demonstrates the ability to create an acid labile chemotherapeutic prodrug using silyl ether chemistry, effective with PRINT nanotechnology.**